A concomitant and complete set of nonvolatile all-optical logic gates based on hybrid spatial solitons

L. L. Columbo,[1,3,*] **C. Rizza,**[1,4] **M. Brambilla,**[2,3]
F. Prati,[1,5] **and G. Tissoni**[6]

[1]*Dipartimento di Scienza e Alta Tecnologia, Università dell'Insubria, via Valleggio 11, Como, I-22100 Italy*
[2]*Dipartimento Interateneo di Fisica, Università degli Studi e Politecnico di Bari, via Amendola 173, Bari, I-70126 Italy*
[3]*Consiglio Nazionale delle Ricerche, CNR-IFN, via Amendola 173, Bari, I-70126 Italy*
[4]*Consiglio Nazionale delle Ricerche, CNR-SPIN, via Vetoio 1, Coppito L'Aquila, I-67100 Italy*
[5]*CNISM, Research Unit of Como, via Valleggio 11, Como I-22100, Italy*
[6]*Institut Non Linéaire de Nice, CNRS, Universitè de Nice Sophia Antipolis, UMR 7335, 1361 Route des Lucioles, Valbonne F-06560, France*
[*]*lorenzo.columbo@gmail.com*

Abstract: We theoretically demonstrate the realization of a complete canonical set of all-optical logic gates (AND, OR, NOT), with a persistent (stored) output, by combining propagative spatial solitons in a photorefractive crystal and dissipative cavity solitons in a downstream broad-area vertical cavity surface emitting laser (VCSEL). The system uses same-color, optical-axis aligned input and output channels with fixed readout locations, while switching from one gate to another is achieved by simply varying the potential applied to the photorefractive crystal. The inputs are Gaussian beams launched in the photorefractive crystal and the output is a bistable, persistent soliton in the VCSEL with a 'robust' eye diagram and large signal-to-noise ratio (SNR). Fast switching and intrinsic parallelism suggest that high bit flow rates can be obtained.

OCIS codes: (190.6135) Spatial solitons; (190.5970) Semiconductor nonlinear optics including MQW; (190.5330) Photorefractive optics.

References and links

1. O. Firstenberg, T. Peyronel, Q. Liang, A. V. Gorshkov, M. D. Lukin, and V. Vuletic, "Attractive photons in a quantum nonlinear medium," Nature **502**, 71–76 (2013).
2. R. Keil, M. Heinrich, F. Dreisow, T. Pertsch, A. Tünnermann, S. Nolte, D. N. Christodulides, and A. Szameit, "All-optical routing and switching for three-dimensional photonic circuitry," Sci. Rep. **1**(94) 1–6 (2011).
3. H. Wei, Z. Wang, X. Tian, M. Käll, and H. Xu, "Cascaded logic gates in nanophotonic plasmon networks," Nat. Commun. **2**(387), 1–5 (2011).
4. T. Kanna and M. Lakshmanan, "Exact soliton solutions of coupled nonlinear Schrödinger equations: Shape-changing collisions, logic gates, and partially coherent solitons," Phys. Rev. E **67**, 046617(2003).
5. S. Barland, J. R. Tredicce, M. Brambilla, L. A. Lugiato, S. Balle, M. Giudici, T. Maggipinto, L. Spinelli, G. Tissoni, T. Knödl, M. Miller, and R. Jäger, "Cavity solitons as pixels in semiconductor microcavities," Nature **419**, 699–702 (2002).
6. P. Genevet, S. Barland, M. Giudici, and J. R. Tredicce, "Cavity soliton laser based on mutually coupled semiconductor microresonators," Phys. Rev. Lett. **101**, 123905 (2008).
7. F. Pedaci, P. Genevet, S. Barland, M. Giudici, and J. R. Tredicce, "Positioning cavity solitons with a phase mask," Appl. Phys. Lett. **89**, 221111 (2006).

#201715 - $15.00 USD Received 22 Nov 2013; revised 13 Jan 2014; accepted 3 Feb 2014; published 18 Mar 2014

8. F. Pedaci, G. Tissoni, S. Barland, M. Giudici, and J. Tredicce, "Mapping local defects of extended media using localized structures," Appl. Phys. Lett. **93**, 111104 (2008).
9. M. Eslami and R. Kheradmand, "All optical logic gates based on cavity solitons with nonlinear gain," Opt. Rev. **19**, 242–246 (2012).
10. T. Maggipinto, M. Brambilla, G. K. Harkness, and W. J. Firth, "Cavity solitons in semiconductor microresonators: Existence, stability, and dynamical properties," Phys. Rev. E **62**, 8726–8739 (2000).
11. R. Landauer, "Irreversibility and heat generation in the computing process," IBM J. Res. Dev. **5**, 183–191 (1961).
12. A. Bérut, A. Arakelyan, A. Petrosyan, S. Ciliberto, R. Dillenschneider, and E. Lutz, "Experimental verification of Landauer's principle linking information and thermodynamics," Nature **483**, 187–190 (2012).
13. L. Columbo, C. Rizza, M. Brambilla, F. Prati, and G. Tissoni, "Controlling cavity solitons by means of photorefractive soliton electro-activation," Opt. Lett. **37**, 4696–4698 (2012).
14. R. McLeod, K. Wagner, and S. Blair, "(3+1)-dimensional optical soliton dragging logic," Phys. Rev. A **52**, 3254–3278 (1995).
15. S. V. Serak, N. V. Tabiryan, M. Peccianti, and G. Assanto, "Spatial soliton all-optical logic gates," IEEE Photonics Technol. Lett. **18**, 1287–1289 (2006).
16. A. Piccardi. A. Alberucci, U. Bertolozzo, S. Residori, and G. Assanto, "Soliton gating and switching in liquid crystal light valve," Appl. Phys. Lett. **96**, 071104 (2010).
17. A. Jacobo, D. Gomila. M. A. Matias, and P. Colet, "Logical operations with localized structures," New J. Phys. **14**, 013040 (2012).
18. M. Peccianti, C. Conti, G. Assanto, A. De Luca, and C. Umeton, "All-optical switching and logic gating with spatial solitons in liquid crystals," Appl. Phys. Lett. **81**, 3335–3337 (2002).
19. H. Enderton, *A Mathematical Introduction to Logic* (Academic 2001).
20. N. Sapiens, A. Weissbrod, and A. J. Agranat, "Fast electroholographic switching," Opt. Lett. **34**, 353–355 (2009).
21. E. DelRe, A. Ciattoni, and E. Palange, "Role of charge saturation in photorefractive dynamics of micron-sized beams and departure from soliton behavior," Phys. Rev. E **73**, 017601 (2006).
22. A. Ciattoni, E. DelRe, A. Marini, and C. Rizza, "Wiggling and bending-free micron-sized solitons in periodically biased photorefractives," Opt. Express **16**, 10867–10872 (2008).
23. M. Brambilla, L. A. Lugiato, F. Prati, L. Spinelli, and W. J. Firth, "Spatial soliton pixels in semiconductor devices," Phys. Rev. Lett. **79**, 2042–2045 (1997).
24. L. Spinelli, G. Tissoni, M. Brambilla, F. Prati, and L. A. Lugiato, "Spatial solitons in semiconductor microcavities," Phys. Rev. A **58**, 2542–2559 (1998).
25. M. Segev and A. J. Agranat, "Spatial solitons in centrosymmetric photorefractive media," Opt. Lett. **22**, 1299–1301 (1997).
26. In all simulations, we used the following parameters: $L_x = 200\mu$m, $L_{PR} = 1$mm, $L_V = 2\mu$m, $\chi = 10^4$, $N_a = 3.04 \cdot 10^{22}\mathrm{m}^{-3}$, $N_d = 101 \cdot N_a$, $n_{PR} = 2.4$, $g = 0.13\mathrm{m}^4\mathrm{C}^{-2}$, $\varepsilon_r = 3 \cdot 10^4$, $\alpha = 5$, $\theta = -2$, $C = 0.45$, $I_p = 2$, $\tau_p = 11.7$ps, $n_V = 3.5$, $\tau_e = 1$ns, $R = 1 - T = 0.996$ and $L_A = 50$nm, $E_{HB}/(E_0\sqrt{T}) = 0.77$
27. S. Gronenborn, J. Pollmann-Retsch, P. Pekarski, M. Miller, M. Strösser, J. Kolb, H. Mönch, and P. Loosen, "High-power VCSELs with a rectangular aperture," Appl. Phys B **105**, 783–792 (2011).
28. E. DelRe, M. Tamburrini, and A. J. Agranat, "Soliton electro-optic effects in paraelectrics," Opt. Lett., **25**, 963–965 (2000).
29. L. M. Surhone, M. T. Timpledon, and S. F. Marseken, *XOR Gate* (Betascript, 2010).
30. E. DelRe, B. Crosignani, and P. Di Porto, "Chapter 3 Photorefractive solitons and their underlying nonlocal physics," Prog. Opt. **53**, 153–200 (2009).
31. X. Hachair, L. Furfaro, J. Javaloyes, M. Giudici, S. Balle, J. Tredicce, G. Tissoni, L. A. Lugiato, M. Brambilla, and T. Maggipinto, "Cavity-solitons switching in semiconductor microcavities," Phys. Rev. A **72**, 013815 (2005).
32. M. Ahmed and M. Yamada, "Effect of intensity noise of semiconductor lasers on the digital modulation characteristics and the bit error rate of optical communication systems," J. Appl. Phys. **104**, 013104 (2008).
33. M. San Miguel and R. Toral, "Stochastic effects in physical systems," in *Nonlinear Phenomena and Complex Systems*, Vol. 5 of Instabilities and Nonequilibrium Structures VI (Kluwer Academic, 2000), pp. 35–127.
34. C. H. Wu, F. Tan, M. K. Wu, M. Feng, and N. Holonyak, "The effect of microcavity laser recombination lifetime on microwave bandwidth and eye-diagram signal integrity," J. Appl. Phys. **109**, 053112 (2011).

1. Introduction

Spatial solitons are the most appealing and investigated carriers for information encoding and processing in photonic devices. In fact nonlinear waves are the phenomena of radiation most endowed with strong and controllable macroscopic interaction which is fundamental in logical computation, while still photon interaction is a formidable task in modern photonics [1]. Confinement and controlled propagation of information carriers is essential for achieving basic operations such as routing, switching and processing in a broad sense; so even when diffraction,

#201715 - $15.00 USD Received 22 Nov 2013; revised 13 Jan 2014; accepted 3 Feb 2014; published 18 Mar 2014

nonlinearity and dispersion are not the keywords, other mechanisms are adopted, as in photonic crystals [2] or plasmonics [3] where the material structure ensures the confined path that light follows in the device, and the steering thereof.

Propagative solitons, such as those occurring in nonlinear crystals of various types (liquid, parametric, photorefractive, etc.) have risen a considerable interest, because their varied and flexible interaction properties are the cornerstone of the processing functionalities [4]. Solitons drifting in each other's wake, or around externally induced modifications of the refraction index, allow to dispatch the carried energy/information to the selected 'output' location, where different interactions produce various gates or operators (copy/fan/etc...). Yet, propagative solitons are intrinsically transient so the results must be stored by resourcing to other optical or opto-electronical means. In addition, intensity thresholds for '0' and '1' must be defined properly and slight drifts of the final soliton destination, as well as soliton distortions due to fluctuations affecting the interaction parameters might result in missing the threshold discriminator.

On the other hand Cavity Solitons (CS) occurring in semiconductors are by now well-established reconfigurable, self-assembled light 'pixels' appearing as bistable intensity peaks in the cross section of the emitted field, self-confined in a homogeneous background (either dark, or of low intensity) [5, 6]. A number of interesting applications in all-optical information processing such as dynamically reconfigurable storage, buffering, material analysis and logic gates [7, 8, 9] have been proposed. CS can be pictured as local attractors of a dissipative extended system, they are intrinsically bistable (i.e. on- and off- switching is ensured by a localized optical addressing leading the system beyond a separatrix [10]) and persistent when the addressing pulse is removed. In particular the dissipative nature of CS complies with a strong boundary in information theory, i.e. that a useful all-optical logic must be capable of yielding a stable, storable, rewritable, output which according to the Landauer principle [11, 12] implies dissipation and entropy production.

Combining electro-activated waveguides in a centrosymmetric photorefractive crystal (PRC) and a broad-area VCSEL, operating at the same wavelength, was the key to recently show how to provide an efficient device for switching and controlling hybrid solitons [13], by-passing the need to optically address the VCSEL from the outside and combining the properties of propagative and dissipative solitons.

When solitons face information processing applications, practical all-optical logic gates need to grant a number of properties [14]. Save for the obvious requirements of speed, low power, phase insensitivity, and parallelism (obvious when using 2D self-confined structures in devices with large aspect ratio) one ought also to ensure that the device inputs, acting as the two logical operands of the gate, and its output, acting as the gate result, belong to the same 'optical line', i.e. have the same propagation direction, wavelength and comparable intensities, so that cascading, fanning, etc. follow naturally. It is not trivial to achieve all these properties simultaneously. For example, in [15, 16] the devices need different wavelengths and orthogonal propagation directions for the input and the output, in [17] different input locations for the two beams corresponding to the operands are required and in [18] different output locations are associated with the results of a single logical operation. Another critical issue is the possibility to achieve operation in the devices as a set of logical gates constituting a functionally complete set; canonically this set is identified as AND, OR and NOT, while NAND and NOR are each a functionally complete set [19]. Of course, for ease of implementation and control, it is desirable that the devices can switch from one gate function to another without modifications of the optical inputs, in intensity/injection time, polarization state or spatial position.

In this paper we propose a scheme based on the same device of [13] where input beam of the same intensity and phase (the issue of phase insensitivity will be discussed in the following) propagate in a PRC and eventually control the switch-on of CS in the VCSEL, exhibiting the

#201715 - $15.00 USD Received 22 Nov 2013; revised 13 Jan 2014; accepted 3 Feb 2014; published 18 Mar 2014

functionality of a canonical set of logical gates. The AND, OR and NOT gates are realized by changing only the bias voltage of the PRC. This control is a global parameter, meaning that it is not a local modification of the system. Also, the whole set of input and output readout channels are fixed in the device. The result of the logical operator corresponds to a CS appearing in the readout locations and it is a permanent (stationary) state of the system; it also has a fixed intensity. We end the paper by discussing the possible performances of the proposed logic gates in terms of SNR, robustness against parameters variation, digital information flow rate.

2. Model for CS formation in a coupled PRC-VCSEL system

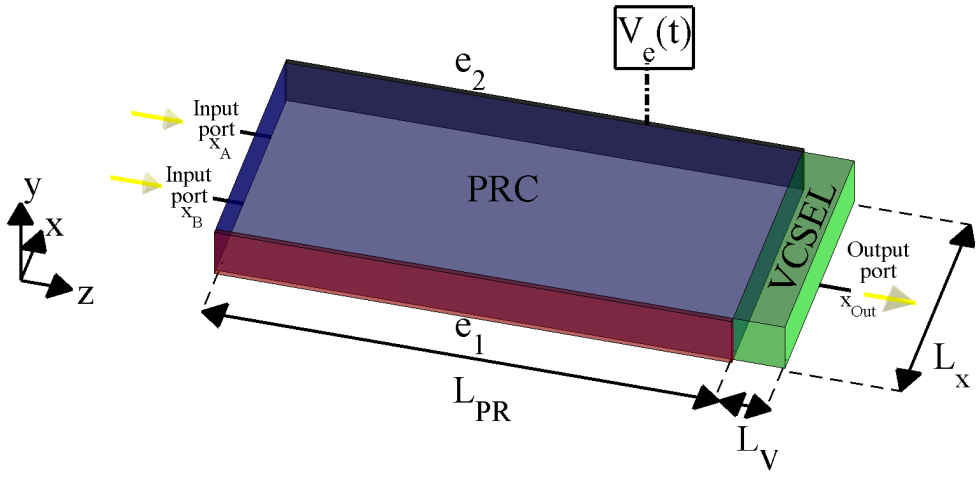

Fig. 1. Schematic of the proposed setup. A centrosymmetric photorefractive crystal PRC is coupled with a broad area VCSEL driven by a spatially uniform field (not shown in the picture). At the 'input ports' infrared Gaussian beams are launched into the PRC and propagate through solitonic waveguides written by using the photorefractive effect and eletroactivated by the potential $V_e(t)$. The latter, applied to the PRC using electrodes $e_{1,2}$ at a distance L_x, allows to control the field intensity and phase landscape at the exit of the PRC on the scale of tens of nanosecond and eventually to switch on a CS in the VCSEL.

Here, we consider the hybrid conservative-dissipative device shown in Fig. 1 and described in [13] where a centrosymmetric PRC is placed in contact with a VCSEL kept slightly below lasing threshold and driven by a coherent, spatially uniform field named *holding beam* (HB).

The proposed set of logical operations is based on the electroactivation of photorefractive solitons in the PRC, which act as waveguides for the propagation of self-confined, interacting beams which in turn generate CSs in the VCSEL. This process consists of two stages: (i) a writing phase at the visible wavelength $\lambda = 0.5$ μm, (ii) a readout at the near-infrared wavelength $\lambda = 0.85$ μm. In the writing phase, when the PRC is not coupled with the VCSEL, a refractive index modulation is encoded in form of two solitonic waveguides exploiting the photorefractive effect in the PRC. In the readout phase two Gaussian beams are launched through the PRC and linearly propagate through the previously imprinted refractive index landscape. The latter can be modified on the scale of tens of nanoseconds [20] by means of the electro-activation potential V_e. In particular the guiding or (anti–guiding) character of

#201715 - $15.00 USD Received 22 Nov 2013; revised 13 Jan 2014; accepted 3 Feb 2014; published 18 Mar 2014

the solitonic channels is determined by the sign of V_e. Depending on the resulting phase and intensity profile at the exit of the PRC a CS can be switched on in the VCSEL. We observe that, contrary to the case discussed in [13], where only a plane wave launched into the PRC was used to both switch on and manipulate CSs, here a spatially uniform external field ($\lambda = 0.85$ μm) is injected into the VCSEL to sustain stable CSs emission after the extinction of the Gaussian beams.

The system dynamics is described by the equations of spatio-temporal field evolution in a paraelectric crystal with bias [21, 22], coupled to those for a VCSEL with external driving [23, 24].

Writing phase

In the writing phase an electromagnetic wave in the visible range (λ=0.5 μm) is launched into an externally biased paraelectric crystal where charges are photo-generated. The charges spatio-temporal dynamics due to diffusion and the applied potential modify the quasi static electric field inside the crystal thus influencing in turn light propagation through the dependence of the refractive index by its intensity. This photorefractive effect is characterized by typical time scale of few seconds.

Formally, the change of the space charge density $\rho(x,z,t)$ in the PRC due to optical photo-excitation and spatial redistribution is given by the charge continuity equation [21, 22]

$$\partial_t \rho = -\mu q \left[\nabla \cdot \left(N_e \mathbf{E}^{(SC)} \right) + \frac{K_B T_{PR}}{q} \nabla^2 N_e \right], \tag{1}$$

where $\nabla = (\partial_x, \partial_z)$, $\mathbf{E}^{(SC)} = (E_x^{(SC)}, E_z^{(SC)}) = -\nabla\phi$ is the space charge field and the quasi-electrostatic potential ϕ satisfies the Poisson equation $\nabla^2\phi = -\rho/(\varepsilon_0\varepsilon_r)$ where ε_0 is the vacuum permittivity and ε_r is the relative static permittivity, μ and q are the electron mobility and charge respectively, K_B is the Boltzmann constant, T_{PR} is the crystal temperature and

$$N_e = \frac{\beta}{2\gamma} \left[\sqrt{(Q - \chi S)^2 + 4\chi Q (N_d/N_a)} - Q - \chi S \right] \tag{2}$$

is the electron density, where N_a and N_d are the acceptor and donor impurity density, respectively. Note that β is the rate of thermal excitation of electrons, γ is the electron-ionized trap recombination rate, $S = 1 + \rho/(qN_a)$, $\chi = \gamma N_a/\beta$, $Q = 1 + |E_{PR}/E_b|^2$, $E_{PR}(x,z,t)$ is the slowly-varying amplitude of the optical electric field polarized along x (at wavelength λ_{PR}=0.5 μm) and E_b is the amplitude of the uniform background illumination. Furthermore, the optical field dynamics is described by [21, 22]

$$i\partial_z E_{PR} + \frac{\partial_x^2 E_{PR}}{2k_{PR}} = -\frac{k_{PR}}{n_{PR}} \delta n E_{PR} \tag{3}$$

$$\delta n = -\frac{1}{2} n_{PR}^3 g \varepsilon_0^2 (\varepsilon_r - 1)^2 [E_x^{(SC)}]^2, \tag{4}$$

where n_{PR} is the uniform background refractive index, $k_{PR} = 2\pi n_{PR}/\lambda_{PR}$, g is the effective electro-optic coefficient and δn is the refractive index change associated with the standard quadratic electro-optic response of paraelectric crystals.

In the description of the readout phase and logic gates operation we will suppose that the profile of the refractive index modulation δn has the form of two solitonic waveguides, encoded in this phase. This can be achieved by applying a potential V_s=10V and injecting into the PRC two Gaussians of shape given by $E_{PR,s}(x, z=0) = E_b \times 1.06 \left(e^{-(x-X_0)^2/2\sigma^2} + e^{-(x+X_0)^2/2\sigma^2} \right)$,

#201715 - $15.00 USD Received 22 Nov 2013; revised 13 Jan 2014; accepted 3 Feb 2014; published 18 Mar 2014

where X_0=20 μm, $\sigma \simeq$10 μm [25]

Readout phase

In the readout phase two near-infrared beams (λ=0.85 μm) are launched and propagate in the PRC. During propagation they acquire an intensity and phase modulation that depends on the refractive index landscape imprinted in the writing phase and on the values of the electroactivation potential. The resulting optical field at the exit of the PRC, because of the coupled PRC/VCSEL configuration, is injected into the driven VCSEL where it represents the CS addressing field.

The dynamical equations describing radiation-matter interaction in the VCSEL are [23, 24]

$$\partial_t E_V = \frac{1}{\tau_p}\Big[-(1+i\theta)E_V + E_I + 2C(1-i\alpha)(N-1)E_V\Big] + i\frac{c}{2k_V n_V}\partial_x^2 E_V \quad (5)$$

$$\partial_t N = -\frac{1}{\tau_e}\left[N - I_p + |E_V|^2(N-1)\right], \quad (6)$$

where $E_V(x,t)$ is the slowly-varying amplitude of the optical electric field polarized along x (at wavelength λ_V=0.85 μm) and scaled to the characteristic amplitude E_0, τ_p is the photon decay time, θ is the cavity detuning between $\omega = 2\pi c/\lambda_V$ and the closest cavity resonance, C is the gain-to-loss ratio, α is the linewidth enhancement factor, N is the carriers density scaled to the transparency value N_0, $k_V = 2\pi n_V/\lambda_V$ and n_V is the background refractive index. In the readout phase, where the PRC and VCSEL are coupled, the injected field E_I is the the sum of the field at the exit of the PRC and the *holding beam* $E_{HB} \in \mathscr{R}$ suitably normalized: $E_I = (E_{HB} + E_{PR}(x, z = L_{PR}, t))/(E_0\sqrt{T})$. The constant E_0 is associated with the saturation intensity $I_0 = \varepsilon_0 c n_V E_0^2/2 = \hbar\omega L_A N_0/(4\tau_e T C)$ where L_A is the length of the region filled by the active medium (generally $I_0 \sim 10\mathrm{KW/cm}^2$), and T is the mirror transmissivity. In the carrier density equation, I_p is the pump current, τ_e is the carriers density decay time and we neglect radiative decay and carriers diffusion.

Here, we have chosen photorefractive parameters associated with a crystal sample of potassium lithium tantalate niobate (KLTN) at room temperature [22] and VCSEL parameters associated with a single longitudinal mode GaAs-GaAlAs laser slightly below threshold [24, 26]. Although the model in Ref.[24] is intrinsically suited for a 2D device such as a VCSEL, we reduced it to a single transverse dimension to deal with the more simple case of 1D solitonic waveguides in the PRC. This is also equivalent of assuming a rectangular VCSEL [27].

In the following section, by integrating the above models we provide a numerical demonstration that CSs formation in this hybrid device allows to implement a complete set of fast, reconfigurable, logic gates. In particular we show that the truth table of the AND, OR and NOT basic gates can be achieved by suitably tuning the global parameter V_e.

3. INPUT and OUTPUT channels definition. Logic operations

In the definition of the input and output channels of the proposed logic gates, we refer to the scheme in Fig. 1.

In the readout phase the inputs operands A and B are represented by two Gaussian beams launched through the imprinted waveguides in the PC at the positions X_A=$-$10 μm and X_B=10 μm

$$\begin{aligned} E_{PR}(x, z=0) &= 0, \quad t < t_0 \\ E_{PR}(x, z=0) &= u_0 e^{-(x-X_{A,B})^2/2\sigma^2 + i\phi}, \quad t_0 \le t \le t_1 \\ E_{PR}(x, z=0) &= 0, \quad t > t_1 \end{aligned} \quad (7)$$

#201715 - $15.00 USD Received 22 Nov 2013; revised 13 Jan 2014; accepted 3 Feb 2014; published 18 Mar 2014

with u_0=0.58$E_0\sqrt{T}$, σ=10 μm, $t_1 - t_0 \simeq$10 ns, ϕ=$\pi/2$ being the phase ϕ referred to the phase of the HB. We assume that $u_0 \neq 0$ in X_A (X_B) corresponds to bit '1' in A (B), while u_0=0 in X_A (X_B) corresponds to bit '0' in A (B). The input beams propagate through the previously imprinted solitonic pattern electroactivated by V_e. At the exit of the PRC the resulting refractive index profile is approximated by [28]

$$\delta n(x, z = L_{PR}) \simeq -\frac{1}{2} n_{PR}^3 g \varepsilon_0^2 (\varepsilon_r - 1)^2 \left(\frac{V_s}{L_x}\right)^2 \left(\frac{1}{1 + \frac{|E_{PR,s}|^2}{|E_b|^2}} - 1 + \frac{V_e}{V_s}\right)^2 . \tag{8}$$

From this saturated Kerr-like response it emerges that the guiding or anti–guiding character of the solitonic channels is determined by the sign of V_e. In particular for negative values of V_e, the radiation is confined around the position X=0 μm. As an example in Fig. 2 we plot the numerically calculated refractive index $\delta n(x,z)$ for $V_e = \pm 37.5$ V. Depending of the choice of V_e the induced modulation of the phase and intensity profile at the PRC exit may or may not switch on a CS in the VCSEL [23]. The output channel OUT, which contains the result of the logical operation, is centered at X_{Out} =0μm, so that the occurrence of a CS in that position is taken as a '1' and '0' otherwise.

According to the results reported in [13], we observe that depending on the phase profile of the input beams at the PRC exit the CS forms and drifts in a final position X_{Out} up to few microns distant from the device center $X = 0$ μm. This would not cause any readout error in the realistic hypothesis that the pick-up area of the readout system (e.g. a photodetector) centered at X=0 μm is typically ~ 100 μm^2.

From the discussion above it is clear that the two beams that represent the 'gates' operands (chosen in phase according to relation (7)) will gain different phases, relative to the HB, so that the total field profile injected into the VCSEL will present intensity peaks that may be appropriate or inappropriate to cause the CS onset. This, in a strict sense, makes our device sensitive to the addressing phases. We note, however, that the phase variation depends on the PRC length and the imprinted refractive index pattern. It is always possible to find a match among these device–dependent quantities so that there exists a significant range of operational parameters for which the field output from the PRC is suited for CS switching.

Finally, as shown in the following, the AND, OR and NOT operations are realized by only changing the bias voltage V_e in the scheme just described, and in this sense we say that they are concomitant.

3.1. Logic operation: AND

To implement the AND gate, we set V_e=$-$37.5 V. For this value of the applied potential the field amplitude and phase at the PRC exit is such that a CS is created and persists ($t \gg t_1$) only if $u_0 \neq 0$ for both the two beams, thus reproducing the truth table of the AND operator. Only the constructive interference of the two input beams that are deviated towards the PRC center by the electroactivated waveguides is able to generate an injected field amplitude $|E_I|$ that locally brings the system beyond the CSs separatrix. In Fig. 3 we plot the field amplitude $|E_{PR}|$ in the PRC (bottom panel), the field amplitude $|E_I|$ injected into the VCSEL (black line in the upper panel) for $t_0 \leq t \leq t_1$, and the field amplitude in the VCSEL at steady state $|E_V|$ (red line in the upper panel). The two different initial conditions correspond to a $(1,1)$ input (left) and to a $(0,1)$ input (right). The $(1,0)$ case is spatially symmetrical with respect to the $(0,1)$ case.

#201715 - $15.00 USD Received 22 Nov 2013; revised 13 Jan 2014; accepted 3 Feb 2014; published 18 Mar 2014

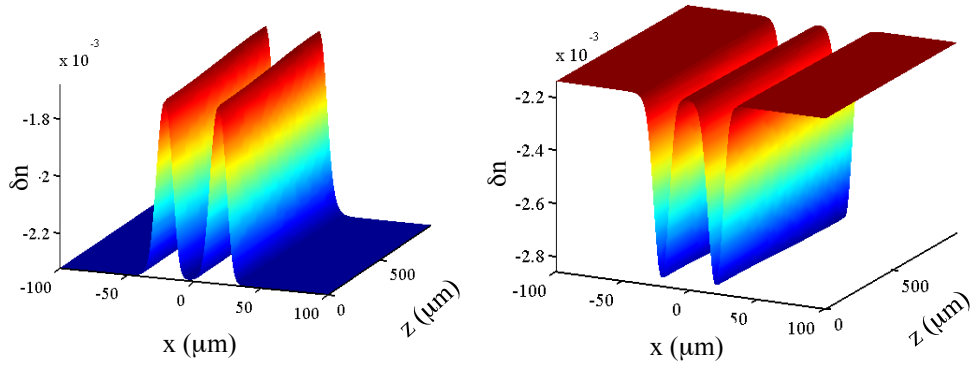

Fig. 2. Numerically calculated refractive index $\delta n(x,z)$ in the PRC for the opposite values V_e=37.5 V (left) and V_e=−37.5 V (right). For negative values of V_e we expect that the injected radiation propagates confined along the PRC center.

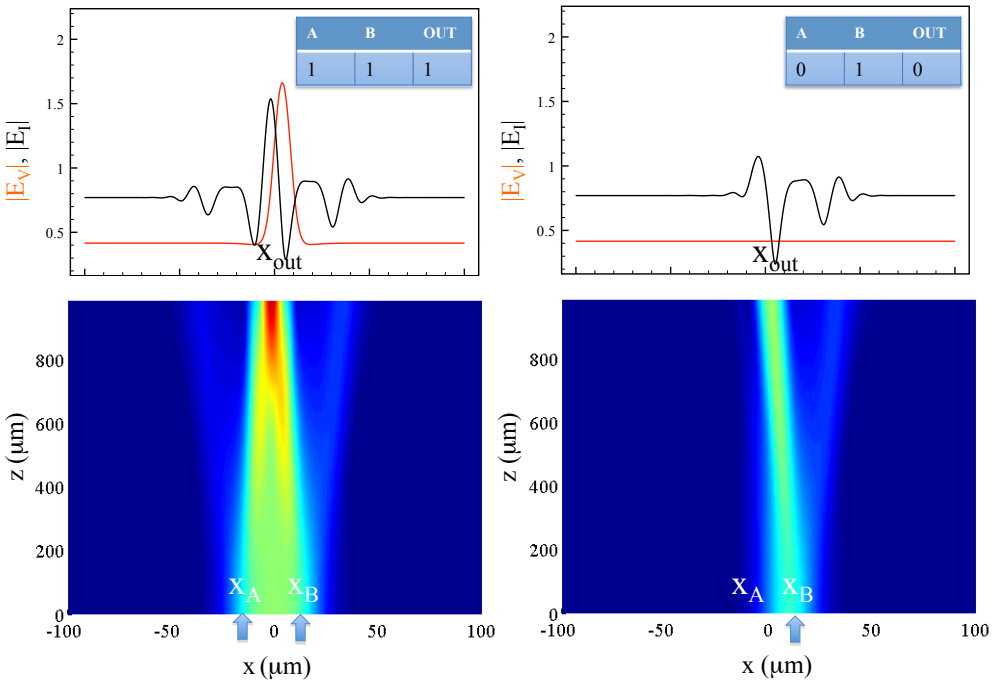

Fig. 3. Logic AND for V_e=−37.5 V. In the bottom panels it is shown the field amplitude in the PRC (in the color scale the dark red corresponds to the maximum amplitude). The black and red lines in the upper panel represent the injected field amplitude and the field amplitude at steady state in the VCSEL respectively. A CS is switched on and persists in X_{Out} if and only if two input Gaussian beams are launched in X_A and X_B. As indicated by the arrows, (left) and (right) refer to the input $(1,1)$ and $(0,1)$ respectively.

3.2. *Logic operation: OR*

The OR gate is implemented by choosing V_e=−42 V as shown in Fig. 4. For this value of the applied potential, the phase and amplitude profile of the field at the PRC exit associated with

#201715 - $15.00 USD Received 22 Nov 2013; revised 13 Jan 2014; accepted 3 Feb 2014; published 18 Mar 2014

a single input Gaussian beam is sufficient to switch on a stable CS, thus reproducing the truth table of the OR operator. As in the previous case, the two input beams sum up constructively during propagation, but even a single input beam injected into the VCSEL becomes a local perturbation capable to switch a CS on.

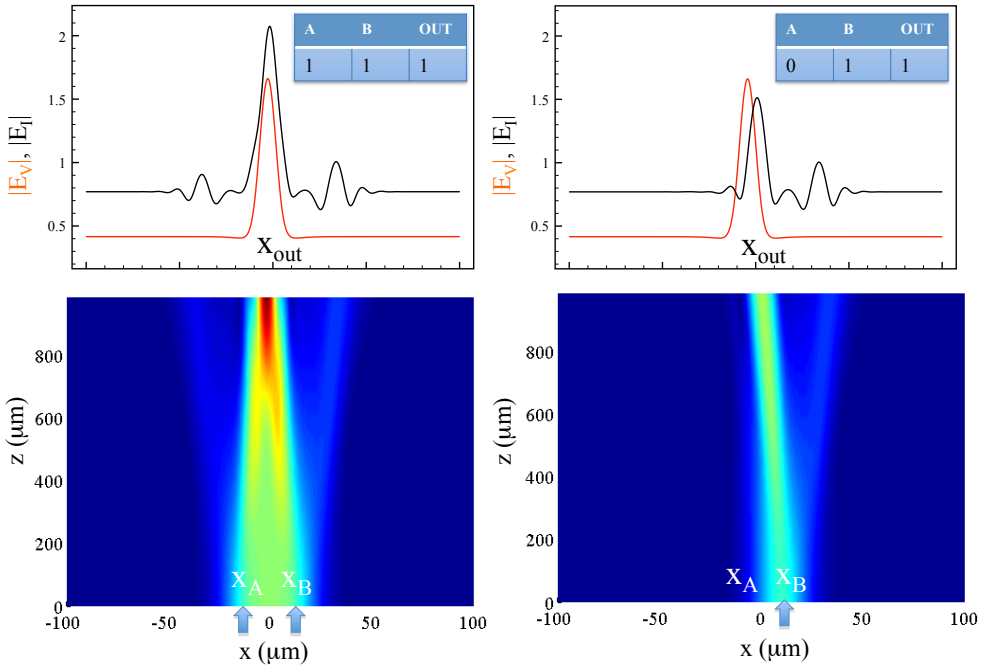

Fig. 4. Logic OR operator for V_e=−42 V. Field amplitude in the PRC and in the VCSEL. The black and red lines in the upper panel represent the injected field amplitude and the field amplitude at steady state in the VCSEL respectively. A CS is switched on and persists in X_{Out} if an input Gaussian beam is launched in X_A or in X_B. As indicated by the arrows, (left) and (right) refer to the input $(1,1)$ and $(0,1)$ respectively.

3.3. Logic operation: NOT (and XOR)

The canonical set is completed by the unary NOT operator that we achieve by choosing $V_e = -40$ V as shown in Fig. 5. The amplitude and phase landscape at the exit of the PRC is such that in presence of an input beam, a stable CS forms in the VCSEL only in absence of the other input beam, thus reproducing the truth table of the NOT operator. In this case the electroactivated waveguides are such that the two input beams interfere destructively during propagation, while a single beam is sufficient to switch a CS on as in the OR gate. To realize a NOT A (NOT B), the value of the input B (A) is always set to '1'. We observe that if we use this scheme as a binary operator, thus letting both inputs A and B to assume values '0' or '1', the gate obtained works as a XOR. The latter combined with the AND and the OR logic gates makes a FULL ADDER, i.e. the digital circuit used to add two binary numbers in any computer [29].

4. Discussion. Logic gates performance

Our simulations assessed that the system performances are robust with respect to variations up to few Volts in the applied potential V_e. The AND gate appears to be most sensitive to the V_e

#201715 - $15.00 USD Received 22 Nov 2013; revised 13 Jan 2014; accepted 3 Feb 2014; published 18 Mar 2014

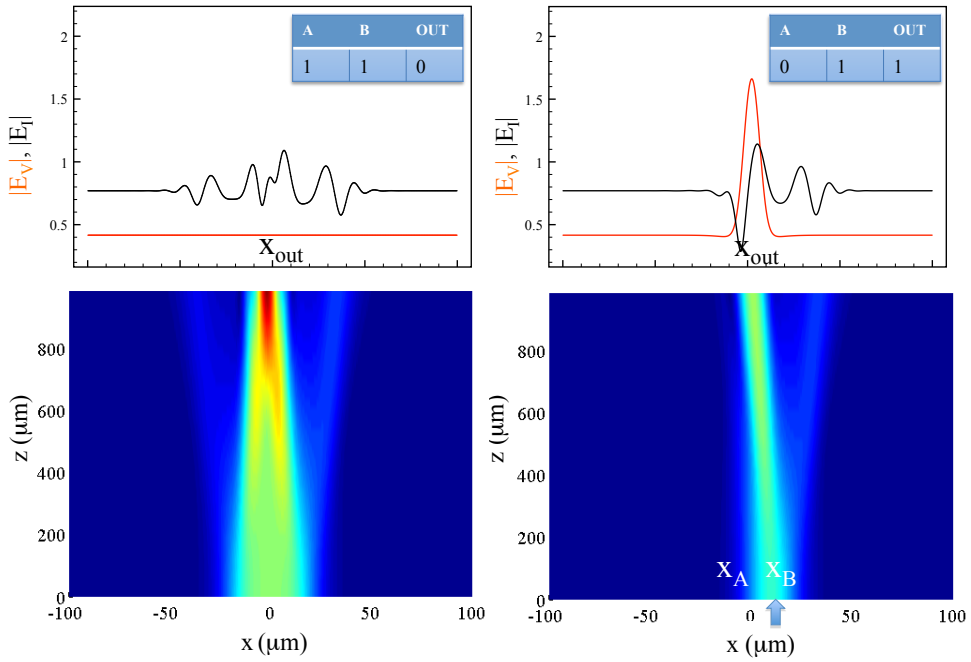

Fig. 5. Logic NOT A operator for $V_e = -40$ V. Field amplitude in the PRC and in the VCSEL. The black and red lines in the upper panel represent the injected field amplitude and the field amplitude at steady state in the VCSEL respectively. A CS is switched on and persists in X_{Out} if an input Gaussian beam is launched in X_B, but not in X_A. As indicated by the arrows, (left) and (right) refer to the input $(1,1)$ and $(0,1)$ respectively.

values and can be achieved within an interval of amplitude 0.3 V (for the input beams parameters used in Figs. 3–5), which is anyway not critical for a properly stabilized electronic control.

The asymmetry in the waveguides shape that is evident in the figures is caused by non-local terms in the modulus square of the space charge field $|E^{SC}|^2$ that affects the refractive index modulations δn and then the solitonic propagation (self-bending) [22, 30]. The nonlocality is linked to the charge migration process in the photorefractive material [22] and have been neglected in the derivation of local Kerr-like relation (8) by assuming a beam size much bigger than the typical scale of the migration process ($< 1\ \mu$m) [30]. The waveguides asymmetry is not critical for the operation of the logic gates that we propose since it induces a slight asymmetry in the injected field phase and intensity at the PRC exit that makes the CS drift towards a final position only few microns away from the central position at $X = 0\ \mu$m we chose as pick-up location [13]. This will not cause any readout error if, as commented above, the pick-up area of the readout system, is sufficiently broad.

Being the output of the operands a stationary CS which is a bistable local attractor of a dissipative extended system [10], the logical '1' and '0' of the output are intrinsically thresholded results, independent of parameter fluctuations (up to a certain fluctuation strength as will be clearer in what follows). This implies that the SNR is high: once the input beam (logical operand levels) impinging onto the PRC are sufficient to switch the CS on in the VCSEL, the logical state of the output will reach an intensity level independent of the pulse intensity and the background noise level will always be considerably smaller than the absolute intensity of the CS.

#201715 - $15.00 USD Received 22 Nov 2013; revised 13 Jan 2014; accepted 3 Feb 2014; published 18 Mar 2014

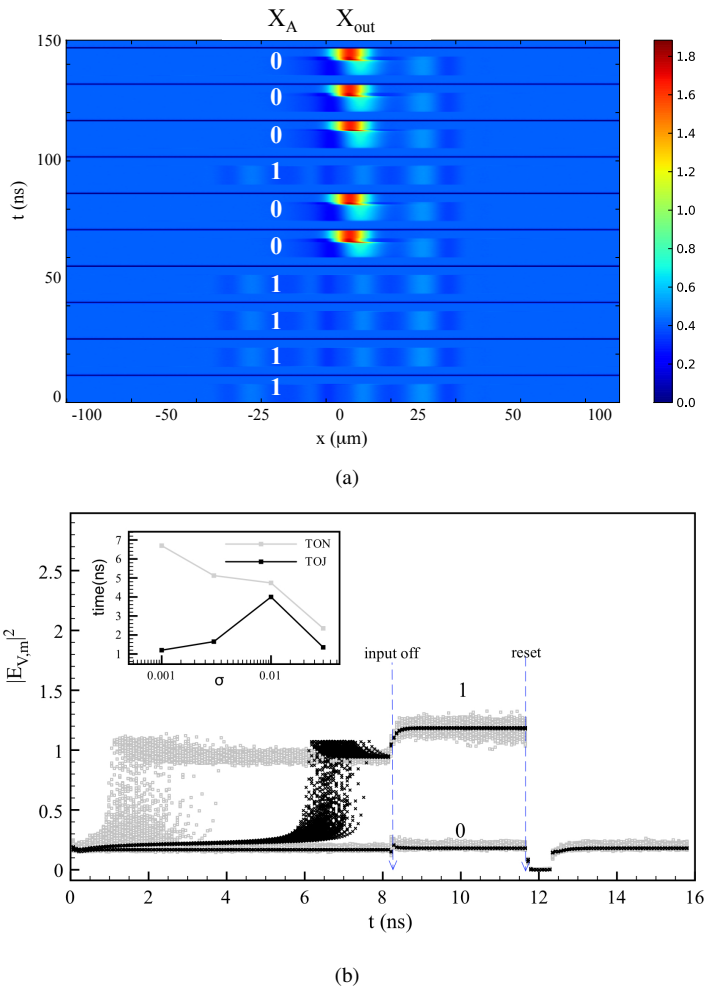

Fig. 6. Eye diagram for a NOT A gate. We plot the electric field intensity in the VCSEL averaged over an interval of $\simeq$20 μm centered at $X = 0$ μm ($|E_{V,m}|^2$) for 300 operation cycles as described in the text. (a) Temporal variation of the electric field amplitude in the VCSEL during a sequence of 10 operation cycles associated with 10 random values of the input A. (b) Eye diagram for the NOT A logic gate in presence of noise with amplitude $\sigma = 0.001$ (black symbols) and $\sigma = 0.03$ (gray symbols). The '0' and '1' output levels are also indicated. In the inset plot the values of the turn-on delay time (TON) and the associated jitter (TOJ) are reported for different noise levels.

Moreover, the logic gates operation speed depends on the on- and off- switching times for the CS, which are of the order of few nanoseconds or less [31], and the waveguide electro-activation characteristic time that can be reduced down to $\sim$10 ns [20]. This yields a perspective bandwidth of $\sim$100 MHz per logical operation in an area of $\sim$1000 μm^2 that corresponds to a potential flux $\sim$100 $GigaOps/(\mathrm{s}\times\ \mathrm{mm}^2)$.

Finally, as a standard tool for a qualitative analysis of the digital system performances, we constructed the eye diagram for the output data stream of the unitary operation NOT A under injection of a bit stream for the input A (we remind that the input B is always equal to '1' in

#201715 - $15.00 USD Received 22 Nov 2013; revised 13 Jan 2014; accepted 3 Feb 2014; published 18 Mar 2014

the NOT A operator). A similar analysis for a solitary semiconductor laser has been recently reported in a case where the direct digital modulation was included in the pump current [32]. Here, a bit stream is generated randomly and then provided to the PRC/VCSEL system as a sequence of pulses according to the definition of the INPUT channels in section 3. In order to collect significant statistics, a total number of 300 operation cycles were produced and the time traces of the field intensity at X_{Out} were superimposed. We note that in order to account for CS drifting towards its steady state location, we plotted the field intensity $|E_{V,m}|^2$ in the VCSEL mediated over an interval of 20 μm centered at $X = 0$ μm. Each operation cycle consists in: 1) assign a value '1' or '0' to the input A by injecting a pulse or not into the PRC, 2) let the VCSEL evolve towards the steady state exhibiting a CS or not and then let the output OUT acquire a logical '1' or '0' value respectively, 3) reset of the output OUT to the '0' level. The reset is obtained by reducing to zero the HB for less than a nanosecond.

In Fig. 6(a) we report for example the electric field amplitude in the VCSEL during a sequence of 10 operation cycles associated with 10 random values of the input A. We observe that, apart from the intrinsic time scale associated with the waveguides electro-activation and the formation of a CS in a VCSEL, the duration of each cycle is affected by the response time of the readout system and the frequency of the shutter or of any other field amplitude modulator used to reset the output. We arbitrarily consider here a total duration of a single cycle of $\sim$15 ns.

As shown in Fig. 6(b), we investigated the influence of the fluctuations in the laser variables E_V and N on the system performances by adding Langevin noise sources $\sigma f(x,t)$ and $\sigma g(x,t)$ into Eqs.(5) and (6) respectively (refer for example to [32]). We assume that the Gaussian noise functions $f(x,t)$ and $g(x,t)$, with zero mean and δ correlation in space and time describe stochastic processes such as as spontaneous emission or pump noise, and field (e.g. HB) fluctuations. To integrate the resulting stochastic differential equations, we used a standard numerical scheme based on modified version of the Runge-Kutta algorithm as described in details for instance in [33].

We note that, a spatially distributed noise term in the HB phase could also be added in order to account for fluctuations in the phase of the input beams respect to the HB, and then may be used to test how strict is the condition of perfect coherence between them. We considered in the following values for sigma: $0.001, 0.003, 0.01, 0.03, 0.1$ of σ (that are almost equally spaced on a $\log_{10}$ scale).

A figure of merit of our digital information processing system can be derived from inspection of Fig. 6(b) where, for sake of clarity, we superimpose only the eye diagrams corresponding to $\sigma = 0.001$ and $\sigma = 0.03$.

- The horizontal opening of the eye diagram, i.e. the interval where the output signal can be sampled with 'fidelity', i.e. where the the '1' or '0' levels can be correctly identified, has a fixed duration starting after the extinction of the input beam at $t = t_1$ and lasting up to the start of the reset phase. Above the CS onset transient (less than $\sim$ 1 ns) it is essentially determined by the response time of the readout device (that we suppose of the order of few nanoseconds) and, instead, not limited by the stochastic dynamics. The widest part of the eye diagram, also called the 'sampling' or 'decision' time, occurs very soon after the extinction of the input signals and the eye width remains about the same for a time that can be in principle much longer than typical readout detector times. This almost fixed amplitude eye diagram is different from those associated with digital systems based on continuos signals, e.g. raised cosine pulses, where the eye opening strongly depend on the shape of the waveforms used to send multiple bits, or equivalently by the transmission bandwidth (see for e.g. Fig. 9 in [34]). A further estimation of the eye diagram quality, and in particular of the eye aperture level, is represented by the signal Q-factor defined

#201715 - $15.00 USD Received 22 Nov 2013; revised 13 Jan 2014; accepted 3 Feb 2014; published 18 Mar 2014

as [32]

$$Q_{signal} = \frac{I_1 - I_0}{\sigma_1 + \sigma_0},$$

where I_j and σ_j, $j = 0, 1$ represent the average intensity and standard deviation of the '0' and '1' levels respectively. The calculated Q_{signal} is high, having a maximum value of $\simeq 200$ for $\sigma = 0.001$ and a minimum value of $\simeq 5$ for $\sigma = 0.03$, and this implies a low probability of incorrect identification of either '1' or '0' (bit error rate).

- The amount of distortion that affects the '1' and the '0' output levels, which is directly linked to the SNR, increases with noise up to the 'closed' eye condition reached for $\sigma = 0.1$. The SNR is defined here as:

$$SNR_j = \frac{I_j}{\sigma_j}.$$

SNR_1 and SNR_0 have their maximum values of $\simeq 25$ db for $\sigma = 0.001$ and their minimum values of $\simeq 10$ db for $\sigma = 0.03$.

- As reported in the inset of Fig. 6(b), by increasing the noise level we also observe a decrease down to the intrinsic limit (i.e. the slow carriers dynamics) of $\simeq 2$ ns in the turn-on delay (TON) time, i.e. the time needed by the VCSEL to reach half of the intensity difference $I_1 - I_0$. This is due to an increase of the average field modulus $|E_I|$ under addition of a noise process. Moreover even the maximum value of $|E_I|$ in each point increases with σ. These two combined effects lead the system closer to the CS separatrix in a shorter time.
  An increased turn-on delay jitter (TOJ), i.e. the standard deviation of the turn-on delay, can be seen in the eye diagram by increasing the noise up to $\sigma = 0.03$. It increases up to a maximum value of $\simeq$4 ns for $\sigma = 0.01$ and it decreases down to $\simeq 1$ ns for $\sigma = 0.03$ (see the inset of Fig. 6(b)). While the TOJ increment is associated with the increase in the amplitude of the noise induced fluctuations in the injected beam modulus and phase, a clear interpretation of the TOJ non monotonic dependence from σ is still object of our study. It might be ascribed to the fact that in absence of the addressing beams a noise amplitude of e.g. $\sigma = 0.03$ is sufficient to bring the system closer to the CS branch. In presence of the Gaussian beams this would change the system trajectories towards the CS branch respect to the cases with smaller σ and then strongly modify the turn-on delay characteristics and the associated jitter.

5. Conclusions

In conclusion, we provide a proof-of-principle demonstration of a complete, all-optical and concomitant set of logical operators (AND,OR, NOT) with persistent output. It is realized by using an hybrid conservative-dissipative device obtained by coupling a centrosymmetric photorefractive crystal with a downstream broad area VCSEL. The proposed set of logical operations is based on the generation process of cavity solitons in the VCSEL trough photorefractive soliton electroactivation in the PRC. The canonically complete set of logical gates exploits the same input and output beams/locations/wavelength/intensities while the switching among the AND, OR and NOT is obtained by only changing the bias voltage of the PRC. The fast semiconductor response and electroactivation process, together with the intrinsic parallelism of structures localization in high Fresnel number devices both allow for a potential flux of $\sim 100\ GigaOps/(\mathrm{s}\times \mathrm{mm}^2$. Robustness against fluctuations in the input parameters is assured by the fixed intensity and the dynamical stability of the output result (formation of a CS). This is also confirmed by

#201715 - $15.00 USD Received 22 Nov 2013; revised 13 Jan 2014; accepted 3 Feb 2014; published 18 Mar 2014

the simulated eye diagram for the logical NOT that shows integrity against noise in terms of low signal distortion, almost constant eye aperture and limited jitter in the CS turn-on delay time.

Acknowledgments

This research has been funded by the Italian Ministry of Research (MIUR) through the Futuro in Ricerca FIRB-grant PHOCOS-RBFR08E7VA and by Progetto DOTE Lombardia. The authors thank Stephane Barland and Eugenio Del Re for fruitful discussions.

#201715 - $15.00 USD Received 22 Nov 2013; revised 13 Jan 2014; accepted 3 Feb 2014; published 18 Mar 2014